

Domain Decomposition Method for Maxwell's Equations: Scattering off Periodic Structures

Achim Schädle¹, Lin Zschiedrich, Sven Burger, Roland Klose¹,
Frank Schmidt

ZIB Berlin, Takustr. 7, D-14195 Berlin, Germany

JCMwave GmbH, Haarer Str. 14a, D-85640 Putzbrunn, Germany

Abstract

We present a domain decomposition approach for the computation of the electromagnetic field within periodic structures. We use a Schwarz method with transparent boundary conditions at the interfaces of the domains. Transparent boundary conditions are approximated by the perfectly matched layer method (PML). To cope with Wood anomalies appearing in periodic structures an adaptive strategy to determine optimal PML parameters is developed.

We focus on the application to typical EUV lithography line masks. Light propagation within the multi-layer stack of the EUV mask is treated analytically. This results in a drastic reduction of the computational costs and allows for the simulation of next generation lithography masks on a standard personal computer.

Key words: domain decomposition, conical diffraction, electro-magnetic scattering, Maxwell's equations, Lithography, EUV, finite elements, perfectly matched layer method

1991 MSC: 65N55

1 Introduction

The fabrication of semiconductor chips is essentially based on an optical projection system. The pattern on a photolithography mask is transferred onto

Email addresses: schaedle@zib.de, lin.zschiedrich@jcmwave.com, sven.burger@jcmwave.com, klose@zib.de, frank.schmidt@zib.de (Frank Schmidt).

¹ Supported by the DFG Research Center MATHEON "Mathematics for key technologies" in Berlin.

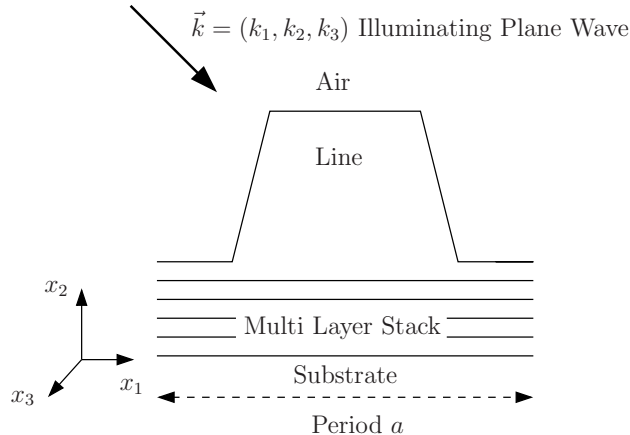


Fig. 1. Layout of an EUV lithography line mask. The structure is periodically repeated in x_1 direction and invariant in x_3 direction. The illuminating light is a plane wave with an arbitrary wave vector $\vec{k} = (k_1, k_2, k_3)$.

the chip by optical projection. State of the art photolithography tools are operated with light of a vacuum wavelength $\lambda \sim 193\text{nm}$, [5]. Currently under development are tools that use extreme ultraviolet light (EUV) with a vacuum wavelength $\lambda \sim 13\text{nm}$. These future systems will contain optical components including multi-layer structures which serve as mirrors. A typical section of an EUV lithography line mask is depicted in Figure 1. The line mask is invariant in x_3 direction and periodic with period a in x_1 direction. The multi-layer stack may consist of more than 100 layers. The thickness of each layer is below a wavelength. The incident wave is twofold oblique – oblique with respect to the mask plane and oblique with respect to the multi-layer structure (conical incident). The polarization of the incident field is arbitrary.

In Section 2 we introduce the mathematical setting of the arising scattering problem and derive the radiating boundary condition in terms of Fourier modes. Further, we show that the exterior Dirichlet as well as Neumann boundary value problem is ill-posed in the presence of so called *Wood anomalies*, [18]. To deal with the large computational domains we propose a domain decomposition method (Section 5). The overall structure is split into sub-domains. The multi-layer sub-domain is treated semi-analytically (c.f. Section 2.2) whereas the other subdomains are discretized by the finite element method utilizing the PML method to approximate transparent boundary conditions. The PML method goes back to Bérenger, [2]. Convergence of the method was proven in [15,16] and [14] for non-periodic problems. As is shown in Section 3 the PML method fails for periodic domains in the presence of Wood anomalies. As a remedy we propose in Section 3.1 a new automatic adaption of the layer size and the spatial discretization within the PML which leads to a quasi infinite layer thickness in the presence of Wood anomalies. In Section 4 we introduce a variational formulation to couple the PML to the interior problem. In contrast to Elschner et al. [11,10] the electromagnetic field $\mathbf{E} = (E_1, E_2, E_3)$

is discretized with higher order Whitney elements for the (E_1, E_2) component and Lagrange elements of the same order in the E_3 component. This allows for the accurate evaluation of Fourier coefficients needed for the coupling to a multi-layer stack as well for the computation of the far field coefficients.

The domain decomposition approach for the wave equation was first studied for the scalar Helmholtz equation. Després and Shaidurov proposed to balance the energy fluxes across domain interfaces for Helmholtz problems, [9,26]. This idea was further expanded, [1,8,7,13,6,12]. Toselli used the PML method at the interfaces of the sub-domains, [27]. This idea is closely related to the ideas of multiple scattering, c.f. [17] with further references. In each sub-domain a simplified scattering problem is solved and the scattered field is added to the incoming field for the neighboring domains. We have recently presented an additive Schwarz algorithm for Helmholtz scattering problems with transparent boundary conditions at the domain interfaces [20]. In this publication we used the DtN operator (Dirichlet to Neumann map). Since the definition of the DtN operator relies on the solvability of the exterior Dirichlet problem a DtN operator may not exist for periodic structures. Hence we avoid the usage of the DtN operator for the formulation of the domain decomposition method in this paper.

The generalization to three dimensional geometries is straightforward.

2 Scattering off periodic line masks

The scattering off a periodic line mask is described by a Maxwell scattering problem, with Bloch-periodic boundary condition in x_1 direction and transparent boundary conditions in x_2 direction. The dependency on the x_3 component is eliminated.

We consider electromagnetic scattering problems governed by the time-harmonic Maxwell's equations

$$\mathbf{curl} \mu^{-1}(\vec{x}) \mathbf{curl} \mathbf{E}(\vec{x}) - \omega^2 \varepsilon(\vec{x}) \mathbf{E}(\vec{x}) = 0, \quad (1a)$$

$$\mathbf{div} \varepsilon(\vec{x}) \mathbf{E}(\vec{x}) = 0, \quad (1b)$$

which may be derived from the Maxwell's equations when assuming a time dependence of the electric field as $\mathbf{E}(\vec{x}, t) = \mathbf{E}(\vec{x}) \exp(-i\omega t)$ with angular frequency ω . The dielectric tensor ε and the permeability tensor μ are L^∞ functions of the spatial variable $\vec{x} = (x_1, x_2, x_3)$. In addition we assume that the tensors ε and μ do not depend on x_3 , that they are periodic functions in x_1 with period a , i.e. $\varepsilon(\vec{x} + (a, 0, 0)) = \varepsilon(\vec{x})$, $\mu(\vec{x} + (a, 0, 0)) = \mu(\vec{x})$, and that they are constant for $x_2 > x_{2,+}$ and $x_2 < x_{2,-}$ with $x_{2,+} > x_{2,-}$. For simplicity

assume that the dielectric and the permeability tensors are isotropic so they may be treated as scalar valued functions. Recall that any solution to (1a) with $\omega \neq 0$ also meets the divergence condition (1b).

A scattering problem may be defined as follows: given an incoming electric field \mathbf{E}_{inc} satisfying the time-harmonic Maxwell's equations (1a) for $x_2 > x_{2,+}$ and $x_2 < x_{2,-}$, compute the total electric field \mathbf{E} , which satisfies (1a) in \mathbb{R}^3 , such that the scattered field $\mathbf{E}_{\text{sc}} = \mathbf{E} - \mathbf{E}_{\text{inc}}$ defined for $x_2 > x_{2,+}$ and $x_2 < x_{2,-}$ meets the radiation condition given in Section 2.1. From a physical point of view, the scattered field has to be outward radiating, so it only transports energy towards infinity.

It is possible to restrict the problem onto a two dimensional strip $[0, a] \times \mathbb{R}$ provided that the incoming field is Bloch periodic in x_1 , [4] and depends harmonically on x_3 , i.e.

$$\mathbf{E}_{\text{inc}}(x_1 + a, x_2, x_3) = \tilde{\mathbf{E}}_{\text{inc}}(x_1, x_2) e^{ik_1 a} e^{ik_3 x_3} \quad (2)$$

where $\tilde{\mathbf{E}}_{\text{inc}}$ is a periodic function in x_1 with period a . The important case of an incoming plane wave meets these restrictions. The total field \mathbf{E} as well as the scattered field are then themselves Bloch periodic in x_1 and depend harmonically on x_3 . This can be seen using a symmetry argumentation where the unique solvability of the scattering problem is assumed.

Below \mathbf{E} , \mathbf{E}_{inc} and \mathbf{E}_{sc} denote the restriction of the respective field onto the strip $[0, a] \times \mathbb{R}$. Let us introduce the domains $\Omega = [0, a] \times [x_{2,-}, x_{2,+}]$, $\Omega_+ = [0, a] \times [x_{2,+}, \infty]$ and accordingly Ω_- . With the definitions

$$\begin{aligned} \mathbf{curl}_3 \mathbf{E} &= (\partial_{x_2} E_3 - ik_3 E_2, ik_3 E_1 - \partial_{x_1} E_3, \partial_{x_1} E_2 - \partial_{x_2} E_1)^T, \\ \mathbf{div}_3 \varepsilon \mathbf{E} &= \partial_{x_1} \varepsilon E_1 + \partial_{x_2} \varepsilon E_2 + ik_3 \varepsilon E_3 \end{aligned}$$

the scattering problem splits into an interior domain problem

$$\begin{aligned} \mathbf{curl}_3 \mu^{-1} \mathbf{curl}_3 \mathbf{E}(x_1, x_2) - \omega^2 \varepsilon \mathbf{E}(x_1, x_2) &= 0 \quad (x_1, x_2) \in \Omega, \\ \mathbf{E}(0, x_2) - \mathbf{E}(a, x_2) e^{ik_1 a} &= 0, \end{aligned} \quad (3)$$

an upper exterior domain problem

$$\begin{aligned} \mathbf{curl}_3 \mu_+^{-1} \mathbf{curl}_3 \mathbf{E}_{\text{sc},+}(x_1, x_2) - \omega^2 \varepsilon_+ \mathbf{E}_{\text{sc},+}(x_1, x_2) &= 0 \quad (x_1, x_2) \in \Omega_+, \\ \mathbf{E}_{\text{sc},+}(0, x_2) - \mathbf{E}_{\text{sc},+}(a, x_2) e^{ik_1 a} &= 0 \end{aligned} \quad (4)$$

and a lower exterior problem on Ω_- of similar type.

Subproblems (3) and (4) are coupled by the following matching conditions on the boundary $x_2 = x_{2,+}$

$$(\mathbf{E} - (\mathbf{E}_{\text{sc},+} + \mathbf{E}_{\text{inc},+})) \times \vec{n}_+ = 0, \quad (5a)$$

$$\left(\mu^{-1} \mathbf{curl}_3 \mathbf{E} - \left(\mu_+^{-1} \mathbf{curl}_3 \mathbf{E}_{\text{sc},+} + \mu_+^{-1} \mathbf{curl}_3 \mathbf{E}_{\text{inc},+}\right)\right) \times \vec{n}_+ = 0, \quad (5b)$$

where $\vec{n}_+ = (0, -1, 0)^T$ denotes the unit normal vector. An analogous condition holds on the boundary $x_2 = x_{2,-}$, coupling the interior and the lower exterior problem.

2.1 Radiation condition for homogeneous exterior domain problem

The exterior domain problems lack a radiation condition. As both upper and lower exterior problem can be treated similarly, we consider the upper exterior domain problem only and drop the '+' . Without loss of generality and to simply matters, we assume that $x_{2,+} = 0$.

Due to the periodicity of $\mathbf{E}_{\text{sc}} \exp(-ik_1 x_1)$ the field has an expansion into Fourier modes

$$\mathbf{E}_{\text{sc}}(x_1, x_2) = e^{+ik_1 x_1} \sum_{n \in \mathbb{Z}} \vec{e}_n(x_2) e^{ix_1 n 2\pi/a}, \quad (6)$$

with the Fourier coefficients

$$\vec{e}_n(x_2) = \frac{1}{a} \int_0^a e^{-ik_1 \xi} \mathbf{E}_{\text{sc}}(\xi, x_2) e^{-i\xi(n2\pi/a)} d\xi .$$

The field $\mathbf{E}_n(x_1, x_2, x_3) = \vec{e}_n(x_2) \exp(i(n2\pi/a + k_1)x_1) \exp(ik_3 x_3)$ is a solution of Maxwell's equations (1a) for $x_2 > 0$. Hence inserting \mathbf{E}_n in (1a) yields

$$\begin{aligned} \mathbf{E}_n(x_1, x_2, x_3) = & \vec{e}_{n,+} e^{i(n2\pi/a + k_1)x_1} e^{ik_{2,n}x_2} e^{ik_3 x_3} + \\ & \vec{e}_{n,-} e^{i(n2\pi/a + k_1)x_1} e^{-ik_{2,n}x_2} e^{ik_3 x_3}, \end{aligned}$$

with $k_{2,n} = \sqrt{k_0^2 - (n2\pi/a + k_1)^2 - k_3^2}$, where the branch cut of the square root is along the negative real axis and $k_0 = \omega \sqrt{\mu \epsilon}$. From this representation it is easily seen that the field can be decomposed into an incoming and an outgoing part.

We have to distinguish three cases:

- (1) $\text{Re } k_{2,n} > 0, \text{Im } k_{2,n} = 0$ (*propagating mode*) Both parts are propagating plane waves with wave vectors $(n2\pi/a + k_1, k_{2,n}, k_3)$ and $(n2\pi/a + k_1, -k_{2,n}, k_3)$ respectively. The second part transports energy in the $-x_2$ direction. We therefore require $\vec{e}_{n,-} = 0$. This corresponds to the well known Sommerfeld radiation condition.

- (2) $\text{Re } k_{2,n} = 0, \text{Im } k_{2,n} > 0$ (*evanescent mode*) The first part is evanescent in x_2 direction while the second part increases exponentially. Therefore we again require $\vec{e}_{n,-} = 0$.
- (3) $k_{2,n} = 0$ (*anomalous mode*) In this case both parts are equal and constant in x_2 direction. Energy is only transported in x_1 and x_3 directions. For the sake of a consistent notation we set $\vec{e}_{n,-} = 0$.

Hence the correct radiation boundary condition is $\vec{e}_{n,-} = 0$ for all $n \in \mathbb{Z}$, such that the Fourier coefficients of the scattered field are given by $\vec{e}_{n,\text{sc}} = \vec{e}_{n,+}$. The anomalous case is rare. For example for $k_1 = 0$ and $k_3 = 0$ it only occurs if $a = 2\pi/(k_0 n)$, hence the wavelength must be a multiple of the period a .

2.1.1 Ill-posed exterior Dirichlet/Neumann boundary value problems

In our previous paper [20] the DtN operator was used to state the coupling between the different domains. However the DtN operator must not exist in the periodic setting – the exterior Dirichlet problem is ill-posed in the presence of anomalous modes.

This may be seen by rewriting Maxwell’s equations separated in Fourier modes. With $\vec{k}_n = (k_1 + n2\pi/a, k_{2,n}, k_3)$ the vectors $\vec{e}_{n,\text{sc}}$ satisfy the algebraic relations

$$-\vec{k}_n \times (\vec{k}_n \times \vec{e}_{n,\text{sc}}) - k_0^2 \vec{e}_{n,\text{sc}} = 0, \quad (7a)$$

$$\vec{e}_{n,\text{sc}} \cdot \vec{k}_n = 0. \quad (7b)$$

The first relation stems from Equation (1a) and the second relation from Equation (1b). If $j \in \mathbb{Z}$ corresponds to an anomalous mode, that is $\vec{k}_j = (k_1 + j2\pi/a, 0, k_3)$, then $\vec{e}_{j,\text{sc}} = (0, 1, 0)$ satisfies (7). Hence $\mathbf{E}_{\text{sc}} = \vec{e}_{n,\text{sc}} \exp(i\vec{k}_j \cdot \vec{x})$ is a solution of the exterior domain problem with zero Dirichlet tangential boundary values. Therefore the Dirichlet boundary value problem is not uniquely solvable. Furthermore due to the divergence condition (7b) the vector $\vec{e}_{j,\text{sc}}$ must be perpendicular to \vec{k}_j . Hence for boundary values with $(d_1, 0, d_3) \cdot \vec{k}_j \neq 0$ the problem is not solvable at all.

By an analogous argument one shows that the Neumann boundary value problem is also ill-posed in the presence of anomalous modes.

2.2 Scattering of an isotropic multi-layer stack – the Transfer Matrix method

The Transfer Matrix method which according to [19] was developed by Schuster [25], will be reviewed here shortly. For more details, the reader is referred to [19,3].

Suppose we are in the situation of Figure 1. Let us consider only the material stack with m finite layers, positioned at $x_{2,j}$, $j = 0, \dots, m$, with $x_{2,j} < x_{2,j+1}$. For $j = 1, \dots, m$ the layer stack is given by the layer thicknesses $x_{2,j} - x_{2,j-1}$, and the material coefficients ϵ_j and μ_j . Additionally for the semi-infinite half-spaces we have ϵ_0, μ_0 and $\epsilon_{m+1}, \mu_{m+1}$. Since the Transfer Matrix algorithm is applied to each Fourier mode $k_{1,n}$ separately we drop the subindex n in this section. In each layer we define the local wave vectors $\vec{k}_j = (k_1, k_{2,j}, k_3)$ and $\overleftarrow{k}_j = (k_1, -k_{2,j}, k_3)$ with $k_{2,j} = \sqrt{\omega^2 \epsilon_j \mu_j - k_1^2 - k_3^2}$ such that $\text{Re } k_{2,j} \geq 0$ and $\text{Im } k_{2,j} \geq 0$. For a given excitation ² from above of the form $\mathbf{E}_{\text{inc}} = A_{m+1,\text{inc}} \exp(i\vec{k}_{m+1}\vec{x}) + B_{m+1,\text{inc}} \exp(i\overleftarrow{k}_{m+1}\vec{x})$ we want to calculate the reflected field $\mathbf{E}_{\text{sc}} = A_{m+1,\text{sc}} \exp(i\vec{k}_{m+1}\vec{x})$. From Snell's law we obtain that the field in each layer is given by $\mathbf{E}_j = A_j \exp(i\vec{k}_j\vec{x}) + B_j \exp(i\overleftarrow{k}_j\vec{x})$. In the lower semi-infinite half space a purely outgoing field is assumed, i.e $A_0 = 0$. In the layers we have $6m$ unknowns – each A or B has 3 components. In the lower semi-infinite domain the only unknowns are the three components of B_0 of the purely outgoing field. In the upper semi-infinite domain there are six unknowns for the excitation and three for the reflected field.

These unknown are determined by the following linear conditions arising from Maxwell's equations: there are $1 + 2 + 2m + 1$ equations from the divergence condition. At the $m + 1$ boundaries of the layers there are $2(m + 1)$ matching conditions for the tangential components of the Dirichlet data and the same number of conditions from matching the Neumann data.

$$\left. \begin{aligned} \mathbf{E}_{j-1} \times \vec{n} &= \mathbf{E}_j \times \vec{n} \\ \mu_{j-1} \mathbf{curl} \mathbf{E}_{j-1} \times \vec{n} &= \mu_j \mathbf{curl} \mathbf{E}_j \times \vec{n} \end{aligned} \right\} \text{ at } \vec{x} = \vec{x}_{j-1} \text{ for } j = 1, \dots, n + 1.$$

Here $\mathbf{E}_0 := \mathbf{E}_{\text{inc}} + \mathbf{E}_{\text{sc}}$. The missing 4 conditions are the tangential components of the Dirichlet and Neumann data of the given incoming field.

This yields a linear system of equations. To avoid large condition numbers due to the complex material tensors, in each layer ansatz functions with amplitude equal to 1 at the layer midpoint are used.

3 Perfectly matched layer method

In the previous section we discussed the homogenous exterior domain problem and derived transparent boundary conditions for each Fourier mode. Transforming back from Fourier space, this boundary condition would be non-local and somehow the anomalous case had to be treated separately. The perfectly matched layer method is an approximate transparent boundary condition, introducing only small reflections that are well under control. The reflections

² Here it is not assumed that the exciting field transports energy only in one direction.

do not occur at the interface of the computational domain and the PML, but stem from the truncation of the PML. Another major advantage of the PML method is, that it fits in the finite-element framework, described shortly in Section 4.1 and thus does not introduce “full” blocks in the discretization.

The PML method is based on a complex continuation of the scattered field. For $\gamma = (1 + i\sigma)$, $\sigma \geq 0$, we define the complex continued field

$$\mathbf{E}_\gamma = \sum_{n \in \mathbb{Z}} \vec{e}_{\text{sc},n} e^{i(n2\pi a + k_1)x_1} e^{ik_{n,2}\gamma x_2} e^{ik_3 x_3}. \quad (8)$$

With the definition

$$\mathbf{curl}_{3,\gamma} \mathbf{E}_\gamma = \left(\frac{1}{\gamma} \partial_{x_2} E_{\gamma,3} - ik_3 E_{\gamma,2}, ik_3 E_{\gamma,1} - \partial_{x_1} E_{\gamma,3}, \partial_{x_1} E_{\gamma,2} - \frac{1}{\gamma} \partial_{x_2} E_{\gamma,1} \right)$$

the field \mathbf{E}_γ satisfies Maxwell’s equations (4) with \mathbf{curl}_3 replaced by $\mathbf{curl}_{3,\gamma}$. In the absence of anomalous modes \mathbf{E}_γ is evanescent for $x_2 \rightarrow \infty$,

$$|\mathbf{E}_\gamma| \leq e^{-\kappa x_2} C,$$

with $\kappa = \min_{n \in \mathbb{Z}} \{\text{Im } k_{n,2}, \sigma \text{Re } k_{n,2}\}$. The idea is to restrict the complex continued exterior domain problem to a truncated domain $\Omega_\rho = [0, a] \times [0, \rho]$ and to impose a zero Dirichlet boundary condition at $x_2 = \rho$. In case κ is small or even 0, i.e. if we are “close” to an anomalous mode a special adaptive PML is used, where the thickness ρ is increased like $1/\kappa$ and the discretization points are distributed with an exponentially increasing mesh width guaranteeing an effective discretization, c.f. Section 3.1. Thus the unbounded exterior problem (4) is replaced by the truncated exterior domain problem

$$\begin{aligned} \mathbf{curl}_{3,\mu_+^{-1}} \mathbf{curl}_3 \mathbf{E}_{\gamma,\rho}(x_1, x_2) - \omega^2 \varepsilon_+ \mathbf{E}_{\gamma,\rho}(x_1, x_2) &= 0 \quad (x_1, x_2) \in \Omega_\rho, \\ \mathbf{E}_{\gamma,\rho}(0, x_2) - \mathbf{E}_{\gamma,\rho}(a, x_2) e^{ik_1 a} &= 0, \\ \mathbf{E}_{\gamma,\rho}|_{x_2=\rho} \times \vec{n} &= 0. \end{aligned} \quad (9)$$

This modified truncated exterior problem is coupled to the interior problem using the modified matching conditions, c.f. (5)

$$(\mathbf{E} - (\mathbf{E}_{\gamma,\rho} + \mathbf{E}_{\text{inc}})) \times \vec{n} = 0, \quad (10a)$$

$$(\varepsilon \mathbf{curl}_3 \mathbf{E} - (\varepsilon_+ \mathbf{curl}_{3,\gamma} \mathbf{E}_{\gamma,\rho} + \varepsilon_+ \mathbf{curl}_3 \mathbf{E}_{\text{inc}})) \times \vec{n} = 0. \quad (10b)$$

Instead of homogenous Dirichlet boundary conditions at $x_2 = \rho$ in (9) one can equally well require that the Neumann data is homogenous, as in the PML the solution is oscillating and exponentially damped.

3.1 Automatic Adaption of PML

Algorithm 1. Adaptive PML method

Require: $\epsilon, \sigma, h_{\text{int}}, \kappa_{\text{min}}$
 Compute $N_{\text{p.w}}$ and ξ_{max} depending on h_{int} and finite element order
while (not converged) **do**
 $\xi_0 = 0.0; \xi_1 = h_{\text{int}}; N = 1;$
 while $(-\ln(\epsilon)/(\xi_N \sigma) < \kappa_{\text{min}})$ **do**
 $\xi_{N+1} = \xi_N + \max\{h_{\text{int}}, 2\pi\sigma\xi_N/(-\ln(\epsilon))/N_{\text{p.w}}\}.$
 if $(\xi_{N+1} > 1/\epsilon)$ **then**
 break
 else
 $N = N + 1$
 end if
end while
 Compute solution u with PML discretization $\{\xi_0, \xi_1, \dots, \xi_N\}$
if $\|u(\cdot, \xi_N)\| \leq \epsilon \|u(\cdot)\|$ **then**
 converged
else if $\xi_N > \xi_{\text{max}}$ **then**
 break
else
 $\kappa_{\text{min}} = \kappa_{\text{min}}/2$
end if
end while

As discussed in Section 2.1 and Section 3 the PML method intrinsically fails in the presence of anomalous modes. For an anomalous mode the field behaves like $\exp(i(k_1 x_1 + k_3 x_3))$ and hence a complex continuation in x_2 direction has no effect on the decay property of the field. To obtain an effective transparent boundary condition we exploit the very specific behavior in x_2 direction of the field and propose a mixed *a priori* and *a posteriori* refinement strategy of the perfectly matched layer method including the automatic adaption of the layer thickness ρ . The algorithm we propose is not restricted to the 2D periodic setting and was first published in [30] We therefore start from a simple generic model. As in our paper [23,29] a prismatoidal coordinate system in the exterior domain with a radial like coordinate ξ and an angular like variable η is used. In the 2D periodic setting ξ is simply the x_2 coordinate and $\eta = x_1$. Another example is a spherical coordinate system in 3D (r, ϕ, θ) with $\xi = r$ and $\eta = (\phi, \theta)$. To proceed we assume the following expansion of the field in the exterior domain

$$\mathbf{u}(\eta, \xi) \sim \int \mathbf{c}(\eta, \alpha) e^{ik_\xi(\alpha)\xi} d\alpha \quad (11)$$

with $\text{Re } k_\xi(\alpha) \geq 0$ and $\text{Im } k_\xi(\alpha) \geq 0$. Hence in ξ direction the field is a superposition of outgoing or evanescent plane waves. In the periodic setting such an expansion is explicitly given in (6).

The complex continuation, $\xi \mapsto \gamma\xi$ with $\gamma = 1 + i\sigma$, gives

$$\|\mathbf{u}_\gamma(\eta, \xi)\| \sim \int \|\mathbf{c}(\eta, \alpha)\| e^{-\kappa\xi} \quad (12)$$

with $\kappa = \sigma \operatorname{Re} k_\xi + \operatorname{Im} k_\xi$.

The PML method only effects the outgoing part with $\operatorname{Re} k_\xi$ strictly larger zero. Field contributions with a large $\operatorname{Re} k_\xi$ component are efficiently damped out. Furthermore evanescent field contributions are damped out independently of the complex continuation. For a proper approximation of the oscillatory and exponential behavior a discretization fine enough is needed to resolve the field. In contrast to that anomalous modes or “near anomalous” modes with $k_\xi \sim 0$ are neither evanescent nor damped out efficiently by the PML. Hence they enforce the usage of a large ρ but can be well approximated with a relatively coarse discretization in ξ due to their smoothness in ξ . These requirements can only be satisfied by using an adaptive discretization. It is useful to think of the complex continuation as a high-frequency filter. With a growing distance ξ to the interior coupling boundary the higher frequency contributions are damped out so that the discretization can be coarsened.

For a given threshold ϵ selected according to the global accuracy requirements as described later we introduce the cut-off function

$$\kappa_{\text{co},\epsilon}(\xi) = -\ln(\epsilon)/\xi.$$

With that at $\xi' > 0$ each component in the expansion (12) with $\kappa > \kappa_{\text{co},\epsilon}(\xi')$ is damped out by a factor smaller than the threshold ϵ ,

$$e^{-\kappa\xi'} < e^{-\kappa_{\text{co},\epsilon}(\xi')\xi} = e^{\ln(\epsilon)} = \epsilon.$$

Assuming that this damping is sufficient we are allowed to select a discretization which must only approximate the lower frequency parts with $\kappa \leq \kappa_{\text{co},\epsilon}(\xi)$ for $\xi > \xi'$. If we use a fixed number $N_{\text{p.w}}$ of discretization points per (generalized) wavelength $2\pi/\kappa$ we get the following formula for the *a priori* determination of the local mesh width $h(\xi) = 2\pi\sigma/\kappa_{\text{co},\epsilon}(\xi)/N_{\text{p.w}}$. A good choice of $N_{\text{p.w}}$ depends on the order of finite element used in ξ -direction and need not to be adapted locally because the field depends smoothly in ξ -direction. Since $\kappa_{\text{co},\epsilon}(\xi) \rightarrow \infty$ for $\xi \rightarrow 0$ the local mesh width would be zero at $\xi = 0$. As it is not reasonable to use a finer discretization in the exterior domain than in the interior domain we bound the local mesh width by the minimum mesh width h_{int} of the interior domain discretization on the coupling boundary,

$$h(\xi) = \max\{h_{\text{int}}, 2\pi\sigma/\kappa_{\text{co},\epsilon}(\xi)/N_{\text{p.w}}\}.$$

The parameters ϵ and $N_{\text{p.w}}$ are also fixed accordingly to the interior domain discretization quality. The grid $\{\xi_0, \xi_1, \xi_2, \dots\}$ is recursively constructed by

$$\xi_{n+1} = \xi_n + h(\xi_n).$$

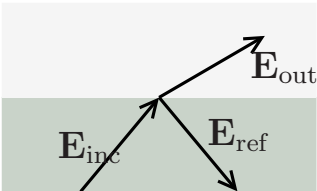


Fig. 2. Test problem for adaptive PML discretization. The lower material has a refractive index equal to $n_{\text{sub}} = 1.5$, the upper material block consists of air ($n_{\text{sup}} = 1.0$). By Snell's law the field is totally reflected for an incident angle equal to the *critical angle* $\vartheta_c = 180 \cdot \arcsin(1.0/1.5)/\pi \approx 41.81$.

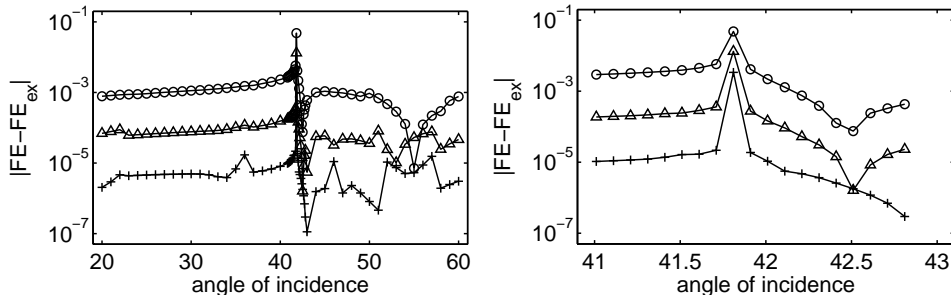


Fig. 3. Left: Field energy error in the interior domain. The three lines (\circ , $\hat{}$, $+$) corresponds to different refinement levels of the interior domain. Right: Zoom into left figure near critical angle.

This way ξ_n grows exponentially with n . To truncate the grid we assume that components in the expansion with $\kappa < \kappa_{\min}$ can be neglected so that the grid $\{\xi_0, \xi_1, \dots, \xi_N\}$ is determined by $\kappa_{\text{co}, \epsilon, \epsilon}(\xi_N) < \kappa_{\min} \leq \kappa_{\text{co}, \epsilon, \epsilon}(\xi_{N-1})$. In the periodic setting there exists such a $\kappa_{\min} > 0$ in case no anomalous mode is present.

As an *a posteriori* control we check if the field is indeed sufficiently damped out at ξ_N , $\|u(\cdot, \xi_N)\| \leq \epsilon \|u(\cdot)\|$.³ Otherwise we recompute the solution with $\kappa_{\min} \rightarrow \kappa_{\min}/2$.⁴ Since for an anomalous mode the field is not damped at all we restrict the maximum ξ_N to $\xi_N < \pi/k_0/\epsilon$. The pseudocode to the algorithm is given in Algorithm 1.

To demonstrate the performance of the adaptive PML algorithm we compute the reflection of a plane wave at a material jump, c.f. Figure 2. We vary the angle of incidence from $\vartheta = 20^\circ$ to $\vartheta = 60^\circ$. Further the incoming field is rotated along the x_3 axis by an angle of 45° , so that the incidence is twofold oblique (conical). Hence the unit direction of the incoming field is equal to $\hat{k} =$

³ Here we assume homogenous Neumann boundary conditions for the truncation of the PML layer. If homogenous Dirichlet boundary conditions are chosen for the truncation of the PML layer, the sufficient damping of the Neumann data may be checked instead.

⁴ This strategy proved useful in many experiment. However we consider to refine it.

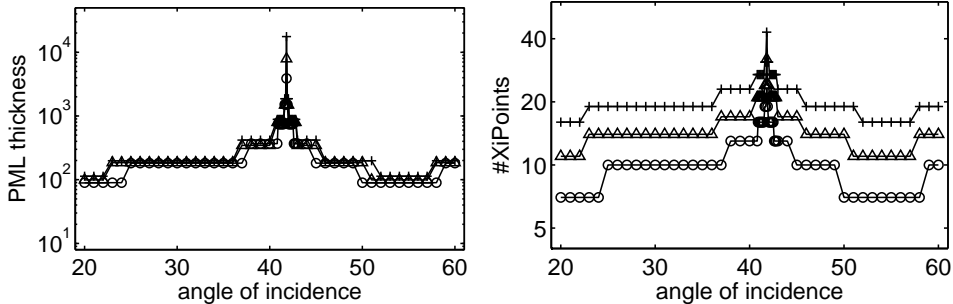


Fig. 4. Left: Thickness of the PML layer. At the critical angle the thickness is up to 10^4 times larger than the diameter of the interior domain. Right: Number of discretization points ξ_j used in the radial direction (x_2). Although the needed thickness of the layer is huge the number of unknowns used in the PML layer remains moderate.

Step	ΔE	$\Delta E'$
0	0.359850	0.335129
1	0.159358	0.166207
2	0.048779	0.049502
3	0.012911	0.012912
4	0.003274	0.003266
5	0.000205	0.000820
6	0.000206	0.000205
7	0.000051	0.000051

Table 1

Convergence of field energy at critical angle of incidence. The first column corresponds to the interior mesh refinement step. The relative error of the electric field energy in the interior domain is given in column two, $\Delta E = \frac{\|\mathbf{E}_{\text{ex}}\|_{L^2}^2 - \|\mathbf{E}_h\|_{L^2}^2}{\|\mathbf{E}_{\text{ex}}\|_{L^2}^2}$. In column three the relative error of the magnetic field energy $\Delta E' = \frac{\|\mathbf{curl} \mathbf{E}_{\text{ex}}\|_{L^2}^2 - \|\mathbf{curl} \mathbf{E}_h\|_{L^2}^2}{\|\mathbf{curl} \mathbf{E}_{\text{ex}}\|_{L^2}^2}$ is given. For fixed PML thickness the solution converges as the interior mesh is refined.

$(\cos 45^\circ \sin \vartheta, \cos \vartheta, \sin 45^\circ \sin \vartheta)$. The interior domain we used has as size of 1.5×1 in wavelength scales. To measure the error we compute the field energy within the interior domain and compare it with the analytic value. In Figure 3 the error is plotted for different refinement levels of the interior domain. The “+” line corresponds to the finest level. In Figure 4 the automatically adapted thickness of the PML is plotted (left) and the number of discretization points N in ξ direction (right). As expected a huge layer is used at the critical angle, whereas the total number of discretization points remains moderate. As can be seen in Figure 3 the maximum error appears at the critical angle. From that one may suspect a failure of the automatic PML adaption. But a closer analysis reveals that the chosen discretization in the PML layer is sufficient

as can be seen from Table 1. Here the thickness of the perfectly matched layer has been fixed and we further refined the interior domain. This way we observe convergence to the true solution but the convergence rate is halved at the critical angle. Hence the maximum error at the critical angle comes from an insufficient interior discretization. We conjecture that this is due to a dispersion effect. Since the wave is traveling along the x_1 direction it reenters the periodic domain leading to large “path length”.

4 Variational form

The coupled problem given by (9), (3) and (10) can be casted into a variational problem on the Sobolev space $H_{0,\rho}(\mathbf{curl}_3, \Omega \cup \Omega_\rho)$ of $H(\mathbf{curl}_3)$ fields with generalized zero Dirichlet values at $x_2 = \rho$.

For a given test function $\Phi \in H_{0,\rho}(\mathbf{curl}_3, \Omega \cup \Omega_\rho)$ the following identity holds true,

$$\begin{aligned} & \gamma \int_{\Omega_\rho} \overline{\Phi} \cdot \mathbf{curl}_{3,\gamma} \mu^{-1} \mathbf{curl}_{3,\gamma} \mathbf{E}_\gamma \\ &= \gamma \int_{\Omega_\rho} \overline{\mathbf{curl}_{3,\gamma} \Phi} \cdot \mu^{-1} \mathbf{curl}_{3,\gamma} \mathbf{E}_\gamma - \int_{x_2=0} \overline{\Phi} \cdot \mu^{-1} \mathbf{curl}_3 \mathbf{E}_{\text{sc}} \times \vec{n}, \end{aligned} \quad (13)$$

where $\mathbf{E}_\gamma(x_1, x_2, x_3) = \mathbf{E}_{\text{sc}}(x_1, \gamma x_2, x_3)$, c.f. (8). We first proof this identity for $\gamma \in \mathbb{R} \setminus \{0\}$. Using the non-euclidian coordinate change

$$T^{-1} : (x_1, x_2, x_3) \mapsto (x_1, \gamma^{-1} x_2, x_3)$$

and applying the transformation rules for differential forms, see [28], one gets

$$\int_{\Omega_{\gamma\rho}} \overline{\Phi^*} \cdot \mathbf{curl}_3 \mu^{-1} \mathbf{curl}_3 \mathbf{E}_{\text{sc}} = \int_{\Omega_\rho} \overline{\Phi_*} \cdot \mathbf{curl}_3 \mu_*^{-1} \mathbf{curl}_3 \mathbf{E}_* \quad \text{and} \quad (14a)$$

$$\int_{\Omega_{\gamma\rho}} \overline{\mathbf{curl}_3 \Phi^*} \cdot \mu^{-1} \mathbf{curl}_3 \mathbf{E}_{\text{sc}} = \int_{\Omega_\rho} \overline{\mathbf{curl}_3 \Phi_*} \cdot \mu_*^{-1} \mathbf{curl}_3 \mathbf{E}_* \quad (14b)$$

with

$$\mu_* = |J| J^{-1} \mu J^{-t} \quad (15a)$$

$$\mathbf{E}_*(x_1, x_2, x_3) = J^t \mathbf{E}_{\text{sc}}(x_1, \gamma x_2, x_3) \quad (15b)$$

$$\Phi_*(x_1, x_2, x_3) = J^t \Phi(x_1, x_2, x_3) = J^t \Phi^*(x_1, \gamma x_2, x_3). \quad (15c)$$

$J = \text{diag}(1, \gamma, 1)$ is the constant Jacobian of T . Note that Φ_* , \mathbf{E}_* are the pulled

back fields to Φ^* and \mathbf{E}_{sc} in the sense of differential form calculus. We have

$$\gamma \int_{\Omega_\rho} \overline{\Phi} \cdot \mathbf{curl}_{3,\gamma} \mu^{-1} \mathbf{curl}_{3,\gamma} \mathbf{E}_\gamma = \int_{\Omega_\rho} \overline{\Phi}_* \cdot \mathbf{curl}_{3\mu_*^{-1}} \mathbf{curl}_3 \mathbf{E}_* \quad (16a)$$

$$\gamma \int_{\Omega_\rho} \overline{\mathbf{curl}_{3,\gamma} \Phi} \cdot \mu^{-1} \mathbf{curl}_{3,\gamma} \mathbf{E}_\gamma = \int_{\Omega_\rho} \overline{\mathbf{curl}_3 \Phi_*} \cdot \mu_*^{-1} \mathbf{curl}_3 \mathbf{E}_* \quad (16b)$$

which is verified by inserting (15) and using $\mathbf{curl}_{3,\gamma} = |\mathbf{J}|^{-1} \mathbf{J} \mathbf{curl}_3 \mathbf{J}^t$. On the other hand integration by parts yields

$$\begin{aligned} & \int_{\Omega_\rho} \overline{\Phi}_* \cdot \mathbf{curl}_{3\mu_*^{-1}} \mathbf{curl}_3 \mathbf{E}_* \\ &= \int_{\Omega_\rho} \overline{\mathbf{curl}_3 \Phi_*} \cdot \mu_*^{-1} \mathbf{curl}_3 \mathbf{E}_* - \int_{x_2=0} \overline{\Phi}_* \cdot (\mu_*^{-1} \mathbf{curl}_3 \mathbf{E}_* \times \vec{n}) \end{aligned} \quad (17)$$

and a respective equation for \mathbf{E}_{sc} , μ , and Φ^* with the domain of integration $\Omega_{\gamma\rho}$. These together with equations in (14) give

$$\int_{x_2=0} \overline{\Phi}_* \cdot (\mu_*^{-1} \mathbf{curl}_3 \mathbf{E}_* \times \vec{n}) = \int_{x_2=0} \overline{\Phi}^* \cdot (\mu^{-1} \mathbf{curl}_3 \mathbf{E}_{\text{sc}} \times \vec{n}) . \quad (18)$$

Using that $\mathbf{E}_\gamma = \mathbf{J}^{-t} \mathbf{E}_*$ and using that the tangential components of Φ^* are equal to Φ , one derives from (16) and (18) the desired identity (13) for real γ . Since each term is a holomorphic function in γ the identity (13) holds true for $\gamma \in \mathbb{C} \setminus \{0\}$.

The coupled problem given by (9), (3) and (10) in weak form is given by

$$\begin{aligned} & \int_{\Omega} \overline{\mathbf{curl}_3 \Phi} \cdot \mu^{-1} \mathbf{curl}_3 \mathbf{E} - \omega^2 \overline{\Phi} \cdot \varepsilon \mathbf{E} + \\ & \gamma \int_{\Omega_\rho} \overline{\mathbf{curl}_{3,\gamma} \Phi} \cdot \mu^{-1} \mathbf{curl}_{3,\gamma} \mathbf{E}_\gamma - \omega^2 \overline{\Phi} \cdot \varepsilon \mathbf{E}_\gamma \\ &= - \int_{x_2=0} \overline{\Phi} \cdot \mu^{-1} (\mathbf{curl}_3 \mathbf{E} - \mathbf{curl}_3 \mathbf{E}_{\text{sc}}) \times \vec{n} \end{aligned} \quad (19)$$

Due to the Neumann coupling condition $\mathbf{curl}_3 \mathbf{E} \times \vec{n} = \mathbf{curl}_3 \mathbf{E}_{\text{sc}} \times \vec{n} + \mathbf{curl}_3 \mathbf{E}_{\text{inc}} \times \vec{n}$ the boundary term is equal to $\int_{x_2=0} \overline{\Phi} \cdot \mu^{-1} \mathbf{curl}_3 \mathbf{E}_{\text{inc}} \times \vec{n}$. This is not yet the basis for a Galerkin ansatz in $H_{0,\rho}(\mathbf{curl}_3, \Omega \cup \Omega_\rho)$ as there is a jump of the Dirichlet data across the boundary $x_2 = 0$, precisely $\mathbf{E}_\gamma + \mathbf{E}_{\text{inc}} = \mathbf{E}|_{x_2=0}$. Let $\Pi(\mathbf{E}_{\text{inc}} \times \vec{n}) \in H_{0,\rho}(\mathbf{curl}_3, \Omega_\rho)$ denote an extension of a field with tangential Dirichlet data equal to $\mathbf{E}_{\text{inc}} \times \vec{n}$ at $x_2 = 0$ to

$H_{0,\rho}(\mathbf{curl}_3, \Omega_\rho)$ and add this to \mathbf{E}_γ to obtain

$$\begin{aligned}
& \int_{\Omega} \overline{\mathbf{curl}_3 \Phi} \cdot \mu^{-1} \mathbf{curl}_3 \mathbf{E} - \omega^2 \overline{\Phi} \cdot \varepsilon \mathbf{E} + \\
& \gamma \int_{\Omega_\rho} \overline{\mathbf{curl}_{3,\gamma} \Phi} \cdot \mu^{-1} \mathbf{curl}_{3,\gamma} (\mathbf{E}_\gamma + \Pi(\mathbf{E}_{\text{inc}} \times \vec{n})) - \omega^2 \overline{\Phi} \cdot \varepsilon (\mathbf{E}_\gamma + \Pi(\mathbf{E}_{\text{inc}} \times \vec{n})) \\
& = - \int_{x_2=0} \overline{\Phi} \cdot \mu^{-1} (\mathbf{curl}_3 \mathbf{E}_{\text{inc}} \times \vec{n}) + \\
& \gamma \int_{\Omega_\rho} \overline{\mathbf{curl}_{3,\gamma} \Phi} \cdot \mu^{-1} \mathbf{curl}_{3,\gamma} \Pi(\mathbf{E}_{\text{inc}} \times \vec{n}) - \omega^2 \overline{\Phi} \cdot \varepsilon \Pi(\mathbf{E}_{\text{inc}} \times \vec{n}) .
\end{aligned} \tag{20}$$

This motivates the definition of the composed field $\mathbf{u} \in H_{0,\rho}(\mathbf{curl}_3, \Omega \cup \Omega_\rho)$ by $\mathbf{u}|_\Omega = \mathbf{E}$ and $\mathbf{u}|_{\Omega_\rho} = \mathbf{E}_{\text{sc}} + \Pi(\mathbf{E}_{\text{inc}} \times \vec{n})$ and of the following bilinear form:

$$a(\Phi, \mathbf{u}) := a_\Omega(\Phi|_\Omega, \mathbf{u}|_\Omega) + a_{\Omega_\rho}(\Phi|_{\Omega_\rho}, \mathbf{u}|_{\Omega_\rho}) \tag{21}$$

with

$$a_\Omega(\Phi, \mathbf{u}) := \int_{\Omega} \overline{\mathbf{curl}_3 \Phi} \cdot \mu^{-1} \mathbf{curl}_3 \mathbf{u} - \omega^2 \overline{\Phi} \cdot \varepsilon \mathbf{u} , \tag{22}$$

$$a_{\Omega_\rho}(\Phi, \mathbf{u}) := \gamma \int_{\Omega_\rho} \overline{\mathbf{curl}_{3,\gamma} \Phi} \cdot \mu^{-1} \mathbf{curl}_{3,\gamma} \mathbf{u} - \omega^2 \overline{\Phi} \cdot \varepsilon \mathbf{u} . \tag{23}$$

With

$$b_\Gamma(\Phi, \Psi) := \int_\Gamma \overline{\Phi} \cdot \mu^{-1} \Psi . \tag{24}$$

we end up with the variational problem: find $\mathbf{u} \in H_{0,\rho}(\mathbf{curl}_3, \Omega \cup \Omega_\rho)$ such that for all $\Phi \in H_{0,\rho}(\mathbf{curl}_3, \Omega \cup \Omega_\rho)$

$$a(\Phi, \mathbf{u}) = a_{\Omega_\rho}(\Phi, \Pi(\mathbf{E}_{\text{inc}} \times \vec{n})) - b(\Phi, \mathbf{curl}_3 \mathbf{E}_{\text{inc}} \times \vec{n}) . \tag{25}$$

Here we have avoided the definition of a DtN-operator. The total field is calculated as the solution of a coupled system (computational domain coupled to the PML), where the Dirichlet and Neumann data enter the equation on the “right-hand side”. If \mathbf{u} is a solution of Maxwell’s equations (1), the integration by parts identity can be rewritten using these bilinear forms as

$$a_\Omega(\Phi, \mathbf{u}) - b(\Phi, -\mathbf{curl}_3 \mathbf{u} \times \vec{n}) = 0 \tag{26}$$

This formula will be useful to represent the Neumann data. Note that in (26) \vec{n} is the “inward” normal with respect to Ω .

4.1 Finite element discretization

To discretize the variational problem (25) we use vectorial finite elements on a triangular mesh in the interior domain and on a quadrilateral mesh in the PML. The three sub-meshes – lower PML mesh, interior domain mesh and

upper PML mesh – fit non-overlapping. In the PML we use a rectangular mesh $[0, x_{1,2}, \dots, a] \times [x_{2,+}, x_{2,+} + \xi_1, \dots, x_{2,+} + \xi_N]$ where ξ_1, \dots, ξ_N are determined as described in Section 3.1. Since the Sobolev space $H_{0,\rho}(\mathbf{curl}_3, \Omega \cup \Omega_\rho)$ is isomorphic to $H_{0,\rho}(\mathbf{curl}_{2D}, \Omega \cup \Omega_\rho) \times H_{0,\rho}^1(\Omega \cup \Omega_\rho)$ with the two dimensional \mathbf{curl} operator $\mathbf{curl}_{2D}(u_1, u_2) = \partial_{x_1}u_2 - \partial_{x_2}u_1$ we use higher order Whitney elements to discretize the first and second component of the electric field and standard Lagrange elements for the third field component of the same order. This finite element space is also used for waveguide mode computations, c.f. [24] and the references therein.

Bloch periodicity is enforced by a multiplication of basis functions associated with one of two corresponding periodic boundaries of the domain by the Bloch factor, c.f. [4]. An interior edge element function remains unchanged, c.f. Figure. 5 (left). The support of a basis function associated with a periodic edge on the boundary consists of two triangles, c.f. Figure. 5 (right). The restriction of the basis function to the left triangle is defined as the standard shape function, whereas the shape-function on the right triangle is multiplied by the Bloch factor $\exp(ik_1a)$. The construction of Bloch periodic Lagrange elements is similar.

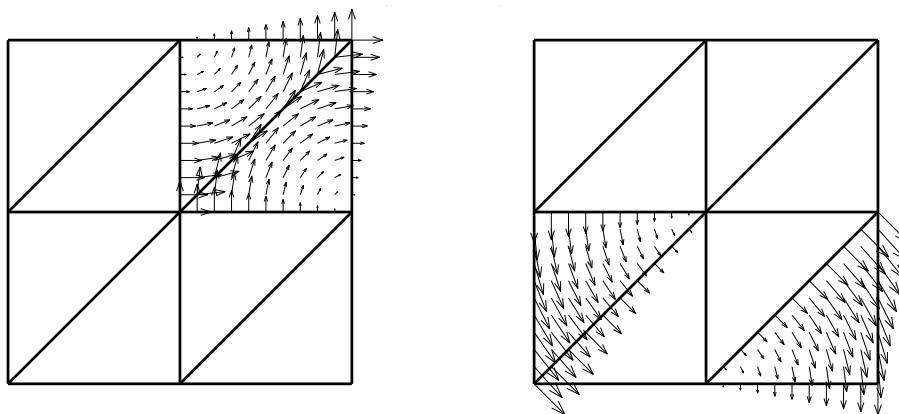


Fig. 5. First order edge elements on a simple grid. In the interior the tangential component is continuous across element boundaries. At the Bloch periodic boundary there is a phase shift.

5 Domain Decomposition Method

The idea for the Schwarz algorithm with transparent boundary conditions at the interfaces is to calculate the solution on every sub-domain separately using transparent boundary conditions and iteratively add the scattered field of each sub-domain to the incoming field for the neighboring sub-domains. The presentation here is restricted to the multiplicative Schwarz-algorithm. In its most general form the domain-decomposition algorithm is given in (27).

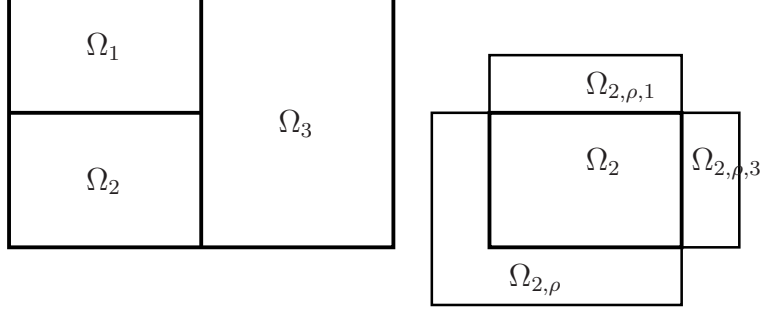


Fig. 6. Schematic sketch of the various domains and PMLs. Left: The computational domain Ω is split in three sub-domains. Right: The sub-domain Ω_2 , with its three different PMLs.

There \mathbf{E}_j^n denotes the n th iterate on sub-domain Ω_j . $\Omega_{j,\rho,i}$ is the PML domain to Ω_j at the interface to Ω_i . and by $\Omega_{j,\rho}$ we denote the PML domain to Ω_j at the interface to the exterior, c.f. Figure 6.

set $\mathbf{E}_j = 0$ for all j

while not converged

for all sub-domains j

find \mathbf{E}_j such that

$$\begin{aligned}
 a_j(\Phi, \mathbf{E}_j) &= a_{\Omega_{j,\rho}}(\Phi, \Pi(\mathbf{E}_{\text{inc}} \times \vec{n})) + \sum_i a_{\Omega_{j,\rho,i}}(\Phi, \Pi(\mathbf{E}_i \times \vec{n})) \\
 &\quad - b_{\Gamma_j}(\Phi, \mathbf{curl}_3 \mathbf{E}_{\text{inc}} \times \vec{n}) - \sum_i b_{\Gamma_{j,i}}(\Phi, \mathbf{curl}_3 \mathbf{E}_i \times \vec{n})
 \end{aligned} \tag{27}$$

$$\forall \Phi \in H_{0,\rho}(\mathbf{curl}_3, \Omega_j \cup \Omega_{j,\rho} \cup_i \Omega_{j,\rho,i})$$

This algorithm requires the evaluation of Neumann data $\mathbf{curl}_3 \mathbf{E}_i \times \vec{n}$ along the boundary. Moreover at cross points, i.e at points given by $\Omega_{j,\rho,k} \cap \Omega_{j,\rho,i} \neq \emptyset$ for $i \neq k$ or $\Omega_{j,\rho,k} \cap \Omega_{j,\rho} \neq \emptyset$, the “incoming” field is not a solution of Maxwell’s equations, as it may have jumps.

This difficulty maybe overcome by choosing sub-domains with a large overlap and by coupling the incoming field to the computational not at the boundary but at some additional artificial boundary in the interior. Here we do not pursue this strategy, but avoid cross-points, by dividing the computational domain horizontally in several sub-domains. Thus the sub-domains are arranged in a linear way. Each sub-domain has only two well separated boundaries neglecting the periodic boundary, and at most two neighboring domains. Inserting an

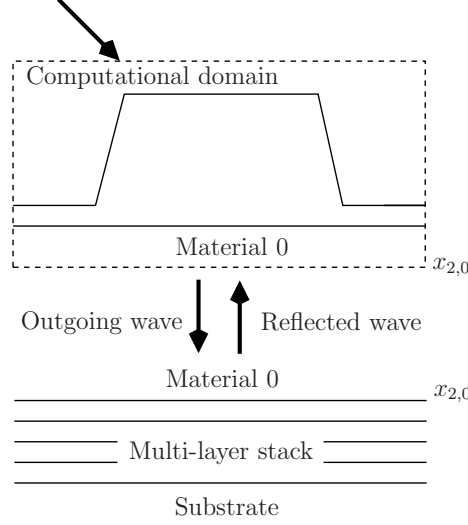


Fig. 7. Decomposition of the problem into two infinite sub-domains. The scattering problem is solved by the Finite Element Method in the upper domain and quasi-analytically in the lower domain.

additional post-processing step, the Neumann-data can be evaluated weakly.

set $\mathbf{E}_j = 0$ for all j

while not converged

for all sub-domains j

find \mathbf{E}_j such that

$$a_j(\Phi, \mathbf{E}_j) = +a_{\Omega_{j,\rho}}(\Phi, \Pi(\mathbf{E}_{\text{inc}} \times \vec{n})) + \sum_i a_{\Omega_{j,\rho,i}}(\Phi, \Pi(\mathbf{E}_i \times \vec{n})) - b_{\Gamma_j}(\Phi, \mathbf{curl}_3 \mathbf{E}_{\text{inc}} \times \vec{n}) - \sum_i b_{\Gamma_{j,i}}(\Phi, \mathbf{curl}_3 \mathbf{E}_i \times \vec{n}) \quad (28)$$

$$\forall \Phi \in H_{0,\rho}(\mathbf{curl}_3, \Omega_j \cup \Omega_{j,\rho} \cup_i \Omega_{j,\rho,i})$$

for all subdomains j

$$\sum_i b_{\Gamma_{j,i}}(\Phi, \mathbf{curl}_3 \mathbf{E}_j \times \vec{n}) + b_{\Gamma_j}(\Phi, \mathbf{curl}_3 \mathbf{E}_j \times \vec{n}) = -a_{\Omega_j}(\Phi, \mathbf{E}_j)$$

In order to distinguish for $k \neq l$ the contribution $b_{\Gamma_{j,k}}(\Phi, \mathbf{curl}_3 \mathbf{E}_j \times \vec{n})$ from, say $b_{\Gamma_{j,l}}(\Phi, \mathbf{curl}_3 \mathbf{E}_j \times \vec{n})$, it is required that there are no test functions that have a support in elements adjacent to $\Gamma_{j,k}$ and $\Gamma_{j,l}$ simultaneously.

5.1 Schwarz algorithm for EUV

For the special application – scattering off an EUV-line mask – one can make use of the “simple” geometry of the double layer stack that serves as a mirror employing the Transfer Matrix algorithm of Section 2.2.

A simple situation is depicted in Figure 7. The upper domain contains the

mask line whereas the lower domain consists of the multi-layer stack and the lower substrate block. Instead of solving Maxwell's equations by the finite element method in the multi-layer stack, the incoming field is Fourier transformed and for each Fourier mode the Transfer Matrix algorithm is used to calculate the scattered field. This can even be simplified. If the tangential component of each Fourier-mode vector field is written as the linear combination of two linear independent polarizations, it is sufficient to compute the reflection coefficients of the multi-layer layer stack for each mode and each polarization only once. The number of Fourier mode ranges from n_{min} to n_{max} . To determine these, we set $k_{max} = 0.1 \cdot 2\pi/h_{max}$, where h_{max} is the maximum segment size of a finite element at the boundary. Then n_{max} is the greatest integer such that $k_1 + n_{max}2\pi/a < k_{max}$, i.e and n_{min} is the greatest integer, such that $k_x - n_{min}2\pi/a > -k_{max}$.

6 Numerical Examples

An academic example

The simple geometry of this example is depicted in Figure 8. It consists of three domains Ω_1 and Ω_2 , each with a quadrilateral material inhomogeneity and Ω_3 a layer stack of four layers below Ω_2 . The period is $a = 1$. The different shadings correspond to different materials as indicated. The permeability is equal to 1 everywhere. The permittivity is given by $\varepsilon_1 = 1.01$, $\varepsilon_2 = 1.52$, $\varepsilon_3 = 1.03$, $\varepsilon_4 = 1.54$, $\varepsilon_5 = 1.55$, $\varepsilon_6 = 1.06$, $\varepsilon_7 = 1.57$, $\varepsilon_8 = 1.08$. The semi-infinite top and lower strips, with refraction indices $\varepsilon_9 = 1$ and $\varepsilon_0 = 1$ are not shown. These are completely modeled by the PML method. Hence there are rather big jumps in the material coefficients at domain interfaces.

The incoming field is a plane waves with wave vector $\vec{k}_{inc} = (1, -2, 1)$ and wave length, $\lambda = 0.84$. The strength is $\vec{s}_{inc} = (1, 1, 1) \times \vec{k}_{inc} / \|(1, 1, 1) \times \vec{k}_{inc}\|$.

In the experiment the relative error is measured against the discrete solution obtained by solving the scattering problem on the whole domain. In solving the the scattering problem on the whole domain, the PML is chosen adaptively. These PML parameters are then fixed and used for all subdomains. Three cases are distinguished.

- (1) Schwarz algorithm with two domains (D2): One domain is Ω_1 and the second domain is the union of Ω_2 and Ω_3 . Thus the layers are discretized by finite elements. In Figure 8 this corresponds to the dark gray lines.
- (2) Schwarz algorithm with two domains (D2-EUV): One domain is Ω_1 , the second domain is Ω_2 . Ω_3 the layer stack is treated analytically and is like

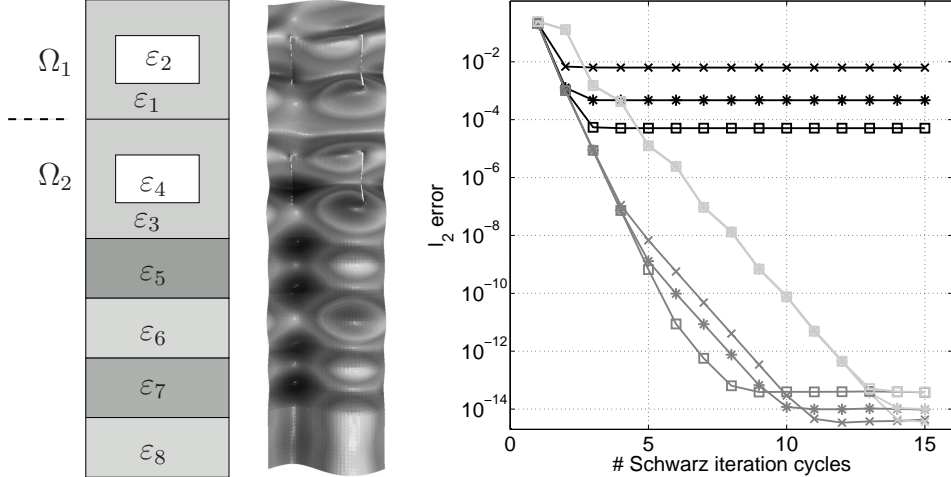


Fig. 8. Material distribution (left) and magnitude of the electric field (middle) for a simple test problem. Convergence plot (right) for $\vec{k}_{\text{inc}} = (1, -2, 1)$, $\lambda = 0.84$ and different refinement levels.

a boundary condition for Ω_2 . That is, if the subproblem on Ω_2 is solved we iterate internally between Ω_2 and Ω_3 and stop if the error is below 10^{-9} or after at most 100 iterations. In the domain decomposition algorithm only the number of iterations between Ω_1 and Ω_2 is counted. In Figure 8 this corresponds to the black lines.

- (3) Schwarz algorithm with three domains (D3): We are using a multiplicative Schwarz algorithm with three subdomains. Within one “iteration cycle”, we first solve for \mathbf{E}_1 , then for \mathbf{E}_2 and finally for \mathbf{E}_3 . In Figure 8 this corresponds to the light gray lines.

For these three cases the error versus the number of Schwarz iteration cycles is shown in Figure 8 (right). The experiment is performed for three different refinement levels, where “x” corresponds to the coarsest level with 5920 degrees of freedom on the whole domain including the PML, the next finer level labeled with “*” is obtained by one uniform refinement of the initial grid and the finest level labeled with “□” by two uniform refinements of the initial grid. In case (D2-EUV) the error saturates at a level that clearly depends on the refinement of the interior grid. This behavior can be expected as the number of Fourier coefficients that are taken into account to couple the layer-stack analytically in the Schwarz iteration is inverse proportional to the mesh-width. In case (D2) and (D3) the error saturates at $1e - 14$, which is close to machine precision. This surprisingly good convergence behavior will be further analyzed in a subsequent paper.

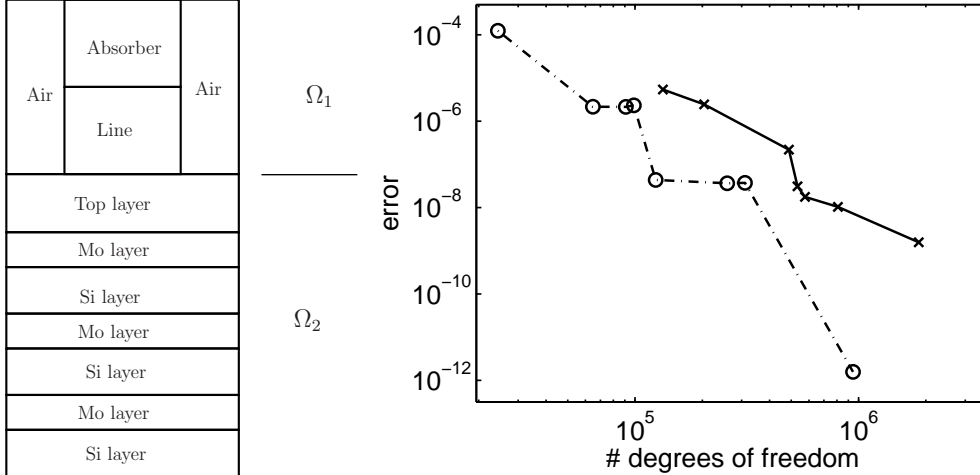


Fig. 9. Left: Sketch of an EUV line mask. Right: Error versus the number of degrees of freedom in finite element mesh. The dashed error curve is obtained using the domain decomposition algorithm, decomposing the computational domain in two sub-domains (the line and the multi-layer stack) and treating the multi-layer stack separately. The solid error curve is obtained discretizing the whole computational domain.

Real life EUV mask

A schematic sketch of a more realistic EUV line mask is shown in Figure 9. There only three out of ten MoSi double layers are shown. The periodicity a is $40nm$. The line made of silicon (Si) and the chromium absorber (Cr) have a width of $20nm$ and a height of $15nm$. The first silicon layer's height is $10nm$. Each molybdenum layer (Mo) has a height of $6nm$ and the subsequent silicon layers have a height of $8nm$. The wavelength is $14nm$. The permeability is 1.0 everywhere. The permittivities are $\varepsilon_{Mo} = 1.69 + 0.016i$, $\varepsilon_{Si} = 1.21 + 0.002i$, $\varepsilon_{Cr} = 1.43 + 0.24i$ and $\varepsilon_{Air} = 1.0$.

Starting from a coarse mesh the grid is pre-refined to have at least 3, 4, 5, 6, 7, 8, 9, 16 and 20 points per wavelength locally. The solution obtained with 20 points per wavelength is taken as a reference solution to measure the error. We use a domain decomposition algorithm and decompose the mask into Ω_1 (line, absorber, air) and Ω_2 (multilayer-stack). The multilayer-stack is treated analytically as described in Section 5.1. Additionally we are using a damping factor of 0.66 in the domain decomposition algorithm to speed up convergence. The PML is chosen adaptively as described in Section 3.1.

Figure 9 shows the error versus the number of degrees of freedom in the finite element grid including the PML. To obtain the solid line, the multi-layer stack is discretized using finite elements. Clearly, if the multi-layer stack is not discretized, but treated analytically and coupled to Ω_1 in the domain-decomposition algorithm, the number of degrees of freedom is reduced drasti-

cally. The above calculations were performed on an *AMD Opeteron PC* with 16GB of RAM. The arising linear system problems are solved with the sparse LU method *PARDISO*, [21,22].

This reduction of the number of degrees of freedom due to the domain decomposition approach, allows to compute realistic masks on standard 32-bit computers.

References

- [1] J.-D. Benamou and B. Després. A domain decomposition method for the Helmholtz equation and related optimal control problems. *J. Comput. Phys.*, 136(1):68–82, 1997.
- [2] J.-P. Bérenger. A perfectly matched layer for the absorption of electromagnetic waves. *J. Comput. Phys.*, 114(2):185–200, 1994.
- [3] M. Born and E. Wolf. *Principles of optics*. Cambridge University Press, 1999.
- [4] S. Burger, R. Klose, A. Schädle, and F. Schmidt and L. Zschiedrich. Adaptive FEM solver for the computation of electromagnetic eigenmodes in 3d photonic crystal structures. In *Proc. Sci. Comp. Electr. Eng. 2004*, 2005.
- [5] S. Burger, R. Köhle, L. Zschiedrich, W. Gao, F. Schmidt, R. März, and C. Nölscher. Benchmark of FEM, Waveguide and FDTD Algorithms for Rigorous Mask Simulation. In J. T. Weed and P. M. Martin, editors, *Photomask Technology*, volume 5992, pages 368–379. Proc. SPIE, 2005.
- [6] X.-C. Cai, M. A. Casarin, F. W. jun. Elliott, and O. B. Widlund. Overlapping Schwarz algorithms for solving Helmholtz’s equation. In J. Mandel, et al., editor, *Domain decomposition methods 10*, volume 218 of *Contemp. Math.*, pages 391–399, 1998.
- [7] F. Collino, S. Ghanemi, and P. Joly. Domain decomposition methods for harmonic wave propagation: a general presentation. *Comput. Methods Appl. Mech. Engrg.*, 184:171–211, 2000.
- [8] A. de La Bourdonnaye, Ch. Farhat, A. Macedo, F. Magoulés, and F.-X. Roux. A non overlapping domain decomposition method for the exterior Helmholtz problem. Technical Report 3271, INRIA, 1997.
- [9] B. Després. Décomposition de domaine et problème de Helmholtz. *C. R. Acad. Sci., Paris, Sér I*, 311(6):313–316, 1990.
- [10] J. Elschner, R. Hinder, F. Penzel, and G. Schmidt. Existence, uniqueness and regularity for solutions of the conical diffraction problem. *Math. Models Methods Appl. Sci.*, 10:317–341, 2000.

- [11] J. Elschner, R. Hinder, and G. Schmidt. Finite element solution of conical diffraction problems. *Advances in Computational Mathematics*, 16:139–156, 2002.
- [12] J. M. Gander, F. Magoulés, and F. Nataf. Optimized Schwarz methods without overlap for the Helmholtz equation. *J. Sci. Comput.*, 24(1):38–60, 2002.
- [13] S. Ghanemi. A domain decomposition method for Helmholtz scattering problems. In *Ninth international Conference on domain decomposition methods*, pages 105–112. DDM.org, 1998.
- [14] T. Hohage, F. Schmidt, and L. Zschiedrich. Solving Time-Harmonic Scattering Problems Based on the Pole ConditionII: Convergence of the PML Method. *SIAM J. Math. Anal.*, 35(3):547–560, 2003.
- [15] M. Lassas and E. Somersalo. On the existence and convergence of the solution of PML equations. *Computing*, 60(3):229–241, 1998.
- [16] M. Lassas and E. Somersalo. Analysis of the PML equations in general convex geometry. In *Proc. Roy. Soc. Edinburgh Sect. A 131*, number 5, pages 1183–1207, 2001.
- [17] P. A. Martin. Multiple scattering: an invitation. In *Third International Conference on Mathematical and Numerical Aspects of Wave Propagation*, pages 3–16, Philadelphia, 1995. SIAM.
- [18] R. Petit. *Electromagnetic Theory of Gratings*. Springer-Verlag, 1980.
- [19] L. Plattner. *A study in biomimetics: nanometer-scale, high-efficiency, dielectric diffractive structures on the wings of butterflies and in the silicon chip factory*. PhD thesis, School of Electronics and Computer Science, University of Southampton, 2003. <http://eprints.ecs.soton.ac.uk/10031/>.
- [20] A. Schädle and L. Zschiedrich. Additive Schwarz method for scattering problems using the PML method at interfaces. Technical Report 05-27, Zuse-Institute Berlin, 2005.
- [21] O. Schenk and K. Gärtner. On fast factorization pivoting methods for symmetric indefinite systems. Technical Report, Computer Science Department, University of Basel, Switzerland, 2004. Submitted.
- [22] O. Schenk and K. Gärtner. Solving unsymmetric sparse systems of linear equations with PARDISO. *Journal of Future Generation Computer Systems*, 20(3):475–487, 2004.
- [23] F. Schmidt. *Solution of Interior-Exterior Helmholtz-Type Problems Based on the Pole Condition Concept: Theory and Algorithms*. Habilitation thesis, Free University Berlin, Fachbereich Mathematik und Informatik, 2002.
- [24] F. Schmidt, T. Friese, L. Zschiedrich, and P. Deuffhard. Adaptive Multigrid Methods for the Vectorial Maxwell Eigenvalue Problem for Optical Waveguide Design. In W. Jäger et al., editor, *Mathematics - Key Technology for the Future: Joint Problems between Universities and Industry*, pages 270–292. Springer, 2003.

- [25] K. Schuster. Anwendung der Vierpoltherapie auf die Probleme der optischen Reflexionsminderung, Reflexionsverstrkung und der Interferenzfilter. *Ann. der Physik, VI. F.*, 4:352–356, 1949.
- [26] V. V. Shaidurov and E. I. Ogorodnikov. Some numerical method of solving Helmholtz wave equation. In G. Cohen, L. Halpern, and P. Joly, editors, *Mathematical and numerical aspect of wave propagation phenomena*, pages 73–79. SIAM, 1991.
- [27] A. Toselli. Some results on overlapping Schwarz methods for the Helmholtz equation employing perfectly matched layers. Technical Report 765, Courant Institute, 1998.
- [28] L. Zschiedrich, S. Burger, R. Klose, A. Schädle, and F. Schmidt. Jcmmode: an adaptive finite element solver for the computation of leaky modes. In Y. Sidorin and C. A. Wächter, editors, *Integrated Optics: Devices, Materials, and Technologies IX*, volume 5728, pages 192–202. Proc. SPIE, 2005.
- [29] L. Zschiedrich, R. Klose, A. Schädle, and F. Schmidt. A new finite element realization of the Perfectly Matched Layer Method for Helmholtz scattering problems on polygonal domains in 2D. *J. Comput Appl. Math.*, 2005. in print; published online.
- [30] Lin Zschiedrich, Sven Burger, Benjamin Kettner, and Frank Schmidt. Advanced Finite Element Method for Nano-Resonators. In in print, editor, *Physics and Simulation of Optoelectronic Devices XIV*. Proc. SPIE, 2006.